Journal of Materials Chemistry A



PAPER

View Article Online
View Journal | View Issue



Cite this: J. Mater. Chem. A, 2023, 11, 9868

Efficient removal of short-chain and long-chain PFAS by cationic nanocellulose†

Although most manufacturers stopped using long-chain per- and polyfluoroalkyl substances (PFASs), including perfluorooctanoic acid (PFOA) and perfluorooctanesulfonic acid (PFOS), short-chain PFASs are still widely employed. Short-chain PFASs are less known in terms of toxicity and have different adsorption behavior from long-chain PFASs. Previous studies have shown electrostatic interaction with the adsorbent to be the dominant mechanism for the removal of short-chain PFASs. In this study, we designed a high charge density cationic guaternized nanocellulose (QNC) to enhance the removal of both short- and long-chain PFASs from contaminated water. Systematic batch adsorption tests were conducted using the QNC adsorbent to compare its efficiency against PFASs with varying chain lengths and functional groups. From the kinetic study, PFBA (perfluorobutanoic acid), PFBS (perfluorobutanesulfonic acid) and PFOS showed rapid adsorption rates, which reached near equilibrium values (>95% of removal) between 1 min to 15 min, while PFOA required a relatively longer equilibration time of 2 h (it obtained 90% of removal within 15 min). According to the isotherm results, the maximum adsorption capacity ($Q_{\rm m}$) of the QNC adsorbent exhibited the following trend: PFOS ($Q_{\rm m}=559~{\rm mg~g^{-1}}$ or 1.12 mmol g^{-1}) > PFOA ($Q_m = 405 \text{ mg g}^{-1}$ or 0.98 mmol g^{-1}) > PFBS ($Q_m = 319 \text{ mg g}^{-1}$ or 1.06 mmol g^{-1}) > PFBS ($Q_m = 319 \text{ mg g}^{-1}$) or 1.06 mmol g^{-1}) g^{-1}) > PFBA ($Q_m = 121 \text{ mg g}^{-1}$ or 0.57 mmol g^{-1}). This adsorption order generally matches the hydrophobicity trend among four PFASs associated with both PFAS chain length and functional group. In competitive studies, pre-adsorbed short-chain PFASs were quickly desorbed by long-chain PFASs, suggesting that the hydrophobicity of the molecule played an important role in the adsorption process on to QNC. Finally, the developed QNC adsorbent was tested to treat PFAS-contaminated groundwater, which showed excellent removal efficiency (>95%) for long-chain PFASs (C7-C9) even at a low adsorbent dose of 32 mg L⁻¹. However, short-chain PFASs (i.e., PFBA and perfluoropentanoic acid (PFPeA)) were poorly removed by the QNC adsorbent (0% and 10% removal, respectively) due to competing constituents in the groundwater matrix. This was further confirmed by controlled experiments that revealed a drop in the performance of QNC to remove short-chain PFASs at elevated ionic strength (NaCl), but not for long-chain PFASs, likely due to charge neutralization of the anionic functional group of PFASs by inorganic cations. Overall, the QNC adsorbent featured improved PFAS adsorption capacity at almost two-fold of PFAS removal by granular activated carbons, especially for short-chain PFASs. We believe, QNC can complement the use of common treatment methods such as activated carbon or ionic exchange resin to remove a wide range of PFAS pollutants, heading towards the complete remediation of PFAS contamination.

Received 28th March 2023 Accepted 18th April 2023

DOI: 10.1039/d3ta01851b

rsc.li/materials-a

1. Introduction

Per- and polyfluoroalkyl substances (PFASs) have been extensively used in various industrial products, such as polymer additives and surfactants, since the 1940s.¹ Due to the presence of multiple strong carbon-fluorine (C-F) bonds, PFASs exhibit high stability and persist in the environment without degradation. Consequently, the issue of PFAS pollution has exacerbated rapidly, and the need to develop effective remediation methods to remove these compounds has caught public and scientific attention. According to a 2019 Environmental Protection Agency

[&]quot;Department of Chemistry, Stony Brook University, Stony Brook, NY 11790, USA. E-mail: arjun.venkatesan@stonybrook.edu; benjamin.hsiao@stonybrook.edu

^bNew York State Center for Clean Water Technology, Stony Brook University, Stony Brook. NY 11794. USA

^cResearch Center for Environmental Changes, Academia Sinica, Taipei 115, Taiwan ^dSchool of Marine and Atmospheric Sciences, Stony Brook University, Stony Brook, NY 11794, USA

[†] Electronic supplementary information (ESI) available. See DOI: https://doi.org/10.1039/d3ta01851b

(EPA) report, as many as 110 million people may have been exposed to PFAS-contaminated drinking water.2 Short-chain PFASs are currently abundant in commerce as they serve as replacement chemicals for phased out long-chain PFASs.3 Shortchain PFASs are defined as molecules with shorter number of C-F units (C \leq 6 for perfluorinated carboxylic acids and C \leq 5 for sulfonic acids).4 Their properties are yet to be fully understood and their effective removal strategies and efficiency are only scarcely reported.5 A recent report indicates that many fast food packaging materials contain a significant amount of total organic fluorine (larger than 100 mg L⁻¹) with perfluorobutanoic acid (PFBA) having the highest concentration (among 30 PFAS targeted compounds tested).6 In another report, the existence of short-chain PFASs is thought to have possible linkage with COVID-19 complications. Several shortchain PFASs, such as perfluorobutane sulfonate (PFBS) and perfluorohexanoate (PFHxA), have already been shown to possess potential reproductive toxicity,8 and some PFAS precursors and alternative PFASs including perfluorooctane sulfonamide (FOSA) and hexafluoropropylene oxide dimer acid (HFPO-DA) may also affect gene expression and alter drug metabolism.9

Among the many remediation methods demonstrated, adsorption is the simplest and most cost-effective approach to remove PFASs. This is because other remediation methods, such as electrochemical oxidation or electron beam, capable of destroying/degrading the PFAS components,10 require complex instrumental setup and intensive energy consumption.11 The incomplete destruction process by these methods can also produce short-chain PFASs that remain harmful.12 Unfortunately, common sorptive materials, such as granular activated carbon (GAC), although suitable to treat hydrophobic and long chain PFASs, exhibit early breakthrough and only mediocre adsorption efficiency for short-chain PFASs.13 The reason is that short-chain PFASs behave less like surfactants and are ineffectively removed by hydrophobic interaction. 14,15 To deal with this, modification of adsorbents with proper cationic functional groups that can provide electrostatic interaction with shortchain PFASs becomes a potential approach. There have been several new sorptive nanomaterials developed that can remove short-chain PFASs with improved efficiency. For example, carbon nanotube (CNT), graphene, zeolites, inorganic metallic nanoparticles, and their composites have been used to remove short-chain PFASs from wastewater and groundwater with some success. 15,16 However, these nanomaterials are not eco-friendly due to their adverse toxicity and possible leaching and they are expensive to manufacture.17 Therefore, there is a need to develop low cost, environmentally friendly and effective nanomaterials, such as nanocellulose-based systems,18 for PFAS

Cellulose is the most abundant biopolymer on Earth. Functionalized cellulose-based adsorbents from cheap feedstocks with low toxicity and biocompatibility are broadly used in many practical water purification treatments.18 However, very limited studies have been reported for PFAS remediation using cellulosic adsorbents.19 To design an effective adsorbent based on the concept of nanocellulose scaffold, we consider two primary PFAS removal mechanisms: (i) hydrophobic attraction between the scaffold and C-F chains, and (ii) electrostatic attraction between the anionic functional groups in PFASs and cationic functional sites on the scaffold. Previously, some groups suggested that electrostatic attraction is the dominant adsorption mechanism for the short-chain PFAS removal, while hydrophobicity is the dominant adsorption mechanism for the long chain PFAS removal.3,5,14

In this study, positively charged quaternized ammonium functionalized nanocellulose or quaternized nanocellulose (QNC) adsorbent was prepared to test our hypothesis that highly charged adsorbents could enhance short-chain PFAS removal. We note that similar microscale quaternized cellulose (QC) adsorbents have been reported for long-chain PFAS removal,20 but the efficacy in QNC (with a significantly higher surface area than QC) for short-chain PFAS removal has yet to be reported. The specific objectives of this study were to: (i) use wood pulp as starting material to synthesize nanoscale QNC through one-step quaternization method, where its degree of functionalization could be adjusted by the etherification process; (ii) evaluate the removal performance of QNC using four model PFASs (perfluorooctanesulfonic acid (PFOS), perfluorooctanoic acid (PFOA), PFBS and PFBA) with different chain length (longchain: C8; short-chain: C4) and charged functional groups (sulfonate and carboxylate) in the targeted contaminants, (iii) probe the mechanisms on PFAS uptake by QNC in the batch system using sorption isotherm and kinetics models; and (iv) further explore the removal mechanisms and understand the effects from different C-F tail lengths and functional groups in PFASs by applying competitive adsorption studies and groundwater tests. We observed that QNC exhibited stronger affinity towards long-chain and sulfonated PFASs compared to short-chain and carboxylated PFASs. The current study confirmed that electrostatic interaction is the major removal mechanism of PFAS by the QNC system, while its hydrophobicity also adds to the adsorption process, resulting in higher adsorption capacity for long-chain PFASs.

2. Experimental methods

2.1. Materials

Never-dried bleached wood pulp was obtained from Domsjo Fabriker, Sweden. The pulp exhibited the hemicellulose content of 4.5% (w/w) and lignin content of 0.6% (w/w) as measured by the R18 test (pulp samples treated with 18% NaOH to dissolve the pulp impurities). Sodium hydroxide (Pellet) was purchased from Macron Fine Chemicals (ACS reagent grade). Hydrochloric acid (36.5-38%) was purchased from VWR Chemical (ACS reagent grade). Glycidyltrimethylammonium chloride (GTMAC) $(\geq 90\%),$ silver nitrate $(\geq 99.0\%),$ fluorooctanesulfonic acid potassium salt (PFOSK) (≥98.0%), nonafluorobutanesulfonic acid (PFBS) (≥97.0%), and heptafluorobutyric acid (PFBA) (≥98.0%) were purchased from Sigma-Aldrich (USA) (analytical or reagent grade). Pentadecafluorooctanoic acid (PFOA) (>98.0%) was purchased from TCI America. Isotopically labeled PFAS internal standards, 13C4-PFBA, ¹³C₃-PFBS, ¹³C₈-PFOA, and ¹³C₈-PFOS, were purchased

from Wellington Laboratories (Guelph, Ontario). LC-MS grade methanol was purchased from Honeywell, USA. Regenerated cellulose syringe filter (pore size of 0.2 $\mu m)$ was purchased from Corning Inc. USA, where a preliminary study was carried out to confirm that there was no filter loss or PFAS releasing. Deionized water was used in all the experiments for preparation of reagents and experimental procedures. PFAS contaminated groundwater samples were collected on Long Island, NY. The water quality parameters and background PFAS concentrations in the Long Island groundwater are shown in Tables S1 and S2, respectively (ESI†).

2.2. Preparation of quaternized nanocellulose (QNC)

The synthesized procedure to prepare QNC was revised from earlier studies. ^{21–23} In brief, 10 g of never-dried wood pulp was mixed with a certain amount of NaOH solution and DI water to achieve the NaOH concentration of 5 wt% and the cellulose fiber suspension at 2.5 wt% or 7.5 wt%. After 30 min stirring at room temperature, GTMAC (glycidyltrimethylammonium chloride) was added at the ratio of 9:1 or 12:1 mol mol ⁻¹ AGU (anhydroglucose unit) as shown in Table 1. The reaction took place at 65 °C for 8 h. To quench the reaction, HCl was added dropwise into the final suspension to neutralize the excess base. Vacuum filtration was used to isolate the reaction mixture, which was washed with DI water several times until the pH became 7.0 to obtain QC. To obtain QNC, around 400 ml 0.3% (w/v) QC suspension in DI water was subjected to GEA Niro Soavi Panada Plus homogenizer at 300 bar for 5 cycles.

2.3. Characterization methods

Fourier-Transform Infrared Spectroscopy (FTIR) was used to investigate the functional groups and chemical bonds on cellulose materials (Text S1†). The crystallinity information was obtained from X-ray Diffraction (XRD) (Text S2†). Conductivity titration (Text S3†), zeta potential measurement (Text S4†) and BET surface area measurement (Text S5†) further characterized the degree of functionalization, charge density and surface area for QNC adsorbent, respectively. To observe and confirm the nanofibrous structure, scanning electron microscope (SEM) and transmission electron microscope (TEM) were also performed to estimate the fiber size and dimension (Text S6†). Details of instrumental information and sample preparation could be found in ESI.†

2.4. PFAS adsorption experiment

Adsorption experiments were conducted to determine the PFAS removal efficiency using the QNC 12:1 sample (in a gel form at

the chosen concentration, Table 1), since this sample contained the highest charge density. Although we considered QNC as an adsorbent, it works more like a coagulant. The presence of QNC suspension/gel (depending on the concentration) can neutralize the negatively charged PFAS molecules and form large aggregates or flocs with strong gel property. In specific, we observed the formation of white flocs after mixing QNC with high concentration of PFAS. These flocs containing PFAS can be efficiently removed from water by conventional low energy microfiltration approaches (*e.g.*, through gravity).

In the kinetic study, an appropriate amount of PFAS solution (5 mg PFAS/L in mg L^{-1}) was mixed with the QNC gel (320 mg L^{-1} for PFBA/PFBS, and 32 mg L^{-1} for PFOA/PFOS) in each experimental vial. The PFAS solution and the QNC gel were well mixed in an orbital shaker operated at 150 rpm, where a small aliquot of sample was taken at different time points from 1 min to 24 h for measurement. In the isotherm study, PFAS solutions with varying initial concentrations (1–50 mg L^{-1} for PFOA and PFOS; 1-100 mg L^{-1} for PFBA; 1-250 mg L^{-1} for PFBS) were measured with the ONC gel at 32 mg L^{-1} (for PFOA and PFOS) or 320 mg L^{-1} (PFBA and PFBS). The adsorbent dose in the isotherm study is the same as that in the kinetic study for each PFAS, where the adsorption time was set as 24 h to make certain that the equilibrium was fully reached. In the competition study, bisolute systems with either PFOS + PFBS or PFOA + PFBA were tested. The initial concentration of PFAS was about 60 mg L^{-1} and the QNC gel concentration was 160 mg L^{-1} . In the displacement study, 60 mg L⁻¹ of PFBA or PFBS was mixed with 160 mg L⁻¹ of QNC gel first and allowed to equilibrate. After 24 h, equal concentration of PFOA or PFOS was spiked into the system. In the ion test, 0.1 M and 1 mM NaCl solutions were added to the QNC/PFAS system separately. PFAS concentrations were set as 2 mg L⁻¹ for PFOS/PFOA with 32 mg L⁻¹ QNC, and 10 mg L^{-1} for PFBS/PFBA with 320 mg L^{-1} QNC (similar to the condition in kinetic study). For the groundwater treatment, increasing dose of QNC gel was added ranging from 32 mg L^{-1} to 640 mg L^{-1} , where the adsorption time was set at 1 h. The pH value was measured as between 3 and 4 for the kinetic, isotherm and competition studies in DI water after adding PFAS, and at 7 for the groundwater adsorption test. A 0.2 µm regenerated cellulose (RC) syringe filter was used to remove all adsorbents after the adsorption study. Control experiments were carried out to confirm that the filter loss of different PFAS on RC filter was negligible.

The filtrate was diluted 1000× or 10 000× with LC-MS grade methanol, and then spiked with isotopically labeled PFAS internal standards (Table S3, ESI†) prior to LC-MS/MS analysis.

Table 1 Preparation of different QNC adsorbents and their functional group contents

Sample	Reaction conditions	GTMAC added amount (mol mol ⁻¹ AGU)	Trimethylammonium chloride content
Raw wood pulp	Unmodified biomass	N.A.	N.A.
QNC 9:1-a	2.5 wt% wood pulp with 5 wt% NaOH at 65 °C for 8 h	9:1	$0.327 \text{ mmol g}^{-1}$
QNC 9:1-b	7.5 wt% wood pulp with 5 wt% NaOH at 65 °C for 8 h	9:1	$0.341 \text{ mmol g}^{-1}$
QNC 12:1	7.5 wt% wood pulp with 5 wt% NaOH at 65 °C for 8 h	12:1	$0.486 \text{ mmol g}^{-1}$

The adsorption experiments were carried out twice to determine the average value and deviation.

2.5. PFAS analysis

PFAS quantification was performed using an Agilent 6495B liquid chromatography tandem mass spectrometer (LC-MS/ MS). The analytical column was Zobrax Eclipse Plus C18 (50 imes3 mm, 1.8 µm) (Agilent, Santa Clara, CA) and a delay column (Agilent Zobrax Eclipse Plus, 50×4.6 mm, $3.5 \mu m$) was placed between the pump and the multi-sampler to minimize any background contamination from solvent, tubing, and pump parts. The aqueous phase was 5 mM ammonium acetate solution (A) and the organic phase was 100% methanol (B). The flow rate was maintained at 0.4 mL min⁻¹ throughout the run and the injection volume was 5 μ L. The initial solvent gradient was set at 90% A and 10% B and maintained for 30 s. The gradient was then ramped from 10% B to 30% B at 2 min, and then further ramped from 30% B to 95% B at 12 min. At the end, the solvent composition was switched to 95% A and equilibrated for 6 min prior to the next injection. Detailed LC-MS/MS operating conditions and corresponding parameters are listed in Table S3 (ESI†). All samples were analyzed in electrospray ionization negative (ESI⁻) mode and data was acquired in a multiple reaction monitoring (MRM) acquisition mode. Two transitions (quantifier and qualifier) were monitored for each PFAS compound except for PFBA (Table S4, ESI†). Agilent Mass-Hunter Quantitative Analysis (B.09.00) was used for data processing.

Results and discussion 3.

3.1. Characterizations of quaternized nanocellulose

Following the green chemistry principle, we used the quaternization modification method to create cationic ONC adsorbents due to its simplicity (i.e., one-pot reaction), less chemical load, and aquatic reaction conditions at a mild temperature. The approach has a good potential to achieve sustainability in producing effective remediations materials with low cost and low toxicity for PFAS removal. To understand the possible optimization pathway for the quaternization modification, we tested two cellulose concentrations: diluted (2.5 wt%) and concentrated (7.5 wt%). Previous studies indicated that there are a few key factors affecting the degree of quaternization, including NaOH concentration and GTMAC addition amount.22,23 It has been reported that the hydroxyl groups on the cellulose surface should be activated by hydroxide ions in order to initiate the nucleophilic addition, in which 5 wt% of NaOH was found to be an appropriate condition to achieve this.²³ If the NaOH concentration is too high, the native cellulose structure can be changed (crystalline conversion can take place). Additionally, the degree of quaternization has been found to be positively correlated with the added GTMAC amount. However, if too much GTMAC is added, the reaction can produce amorphous cellulose derivates and destruct the microfibril structure.22,23 Another side reaction is the hydrolysis of GTMAC, which can yield non-reactive reagent and thus decrease the degree of substitution.24 The resulting QNC samples and corresponding characterization results are summarized in Table 1. Based on this study, we found that the QNC 12:1 sample created by the cellulose condition of 7.5 wt% and the highest GTMAC content used (12:1) created the highest cationic charge, which we used for the adsorption study in this work.

The functional groups for raw wood pulp and varying QNC samples were confirmed from the FTIR spectra. As seen in Fig. 1a, all samples exhibited signature cellulose peaks at a region from 500 to 1400 cm^{-1} (e.g., the intense pyranose ether band at 1050 cm⁻¹, the broad peak between 3200 to 3500 cm⁻¹ from the -OH groups of the cellulose scaffold). Most importantly, we observed that the appearance of a new peak at 1480 cm⁻¹ in all QNC samples, that could be attributed to the trimethyl group of quaternary ammonium.22 Additionally, the peak at 1640 cm⁻¹ might be due to the vibration of quaternary nitrogen bond or bound water, which was seen for both QNCs

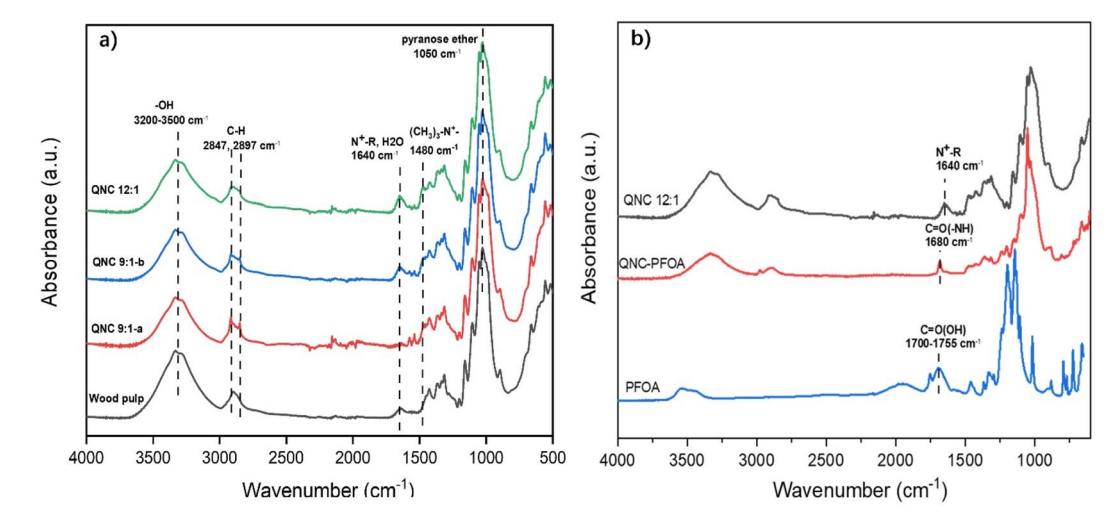


Fig. 1 (a) The FTIR spectra for raw wood pulp, and three QNC samples (QNC 9:1-a, 9:1-b and 12:1); (b) Comparison of QNC 12:1, QNC-PFOA and PFOA.

and wood pulp, respectively. The peak at 2897 cm⁻¹ for wood pulp fragmented into two small peaks might be due to the addition of quaternary ammonium group, which could be assigned to the out-of-plane bending of the C-H stretching in methyl group.²³ The spectra in Fig. 1a indicate the successful incorporation of trimethyl quaternary ammonium groups on the cellulose backbone. Additionally, we measured the QNC sample after PFOA adsorption and compared that with the spectra of PFOA and neat QNC (Fig. 1b). It was seen that a new peak appeared at 1680 cm⁻¹, which could be assigned to the amide I vibration from the CO-NH bond.^{25,26} This observation supports the augment that the carboxylate group on PFOA can interact with the quaternary ammonium group on QNC through electrostatic interaction.

For the cellulose and QNC morphology analysis, we used both SEM and TEM techniques, and the results are shown in Fig. 2. SEM images show partially defibrillated fibers (Fig. 2c and d) for ONC 12:1 when compared with wood pulp fibers (Fig. 2a and b). Overall, the pulp fibers were thicker in size and they were interlocked with each other (Fig. 2a and b), whereas some thinner individual fibers were observed on QNC (Fig. 2c and d). This could be due to the homogenization process of QNC slurry, which resulted in defibrillation of microfibers into nanofibers due to the charge repulsion. TEM images confirmed that after homogenization, QNC contained mainly the nanofiber form (Fig. 2e and f). The average fiber dimensions of QNC 12:1 measured from the TEM images were 110 \pm 57 nm in length and 6.5 ± 1.4 nm in width. However, we noted that some part of QNC 12:1 contained partially defibrillated morphology (observed as swollen microfibers). Nevertheless, the overall surface area in ONC is significantly larger than that of unmodified wood pulp in Table 2.

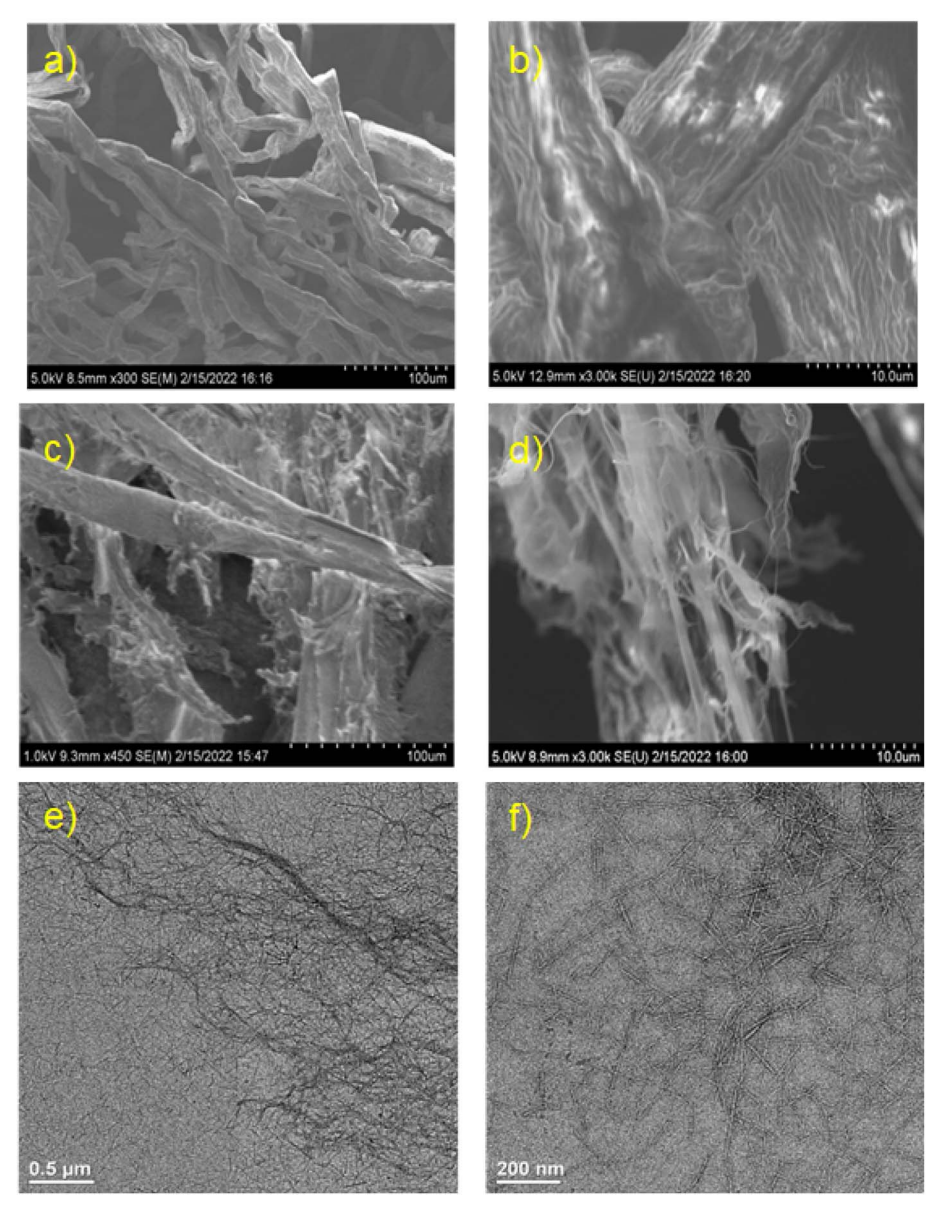


Fig. 2 SEM images for air-dried wood pulp fiber (a and b) and freeze-dried QNC 12:1 (c and d). TEM images for QNC 12:1 (e and f).

Table 2 Characterization results for different QNC adsorbents

Sample	Crystallinity index (CI value)	Zeta potential value	BET surface area
Wood pulp	77%	-20.3 mV	6.10 m ² g ⁻¹
QNC 9:1-a	77%	27.9 mV	21.62 m ² g ⁻¹
QNC 9:1-b	76%	36.0 mV	72.17 m ² g ⁻¹
QNC 12:1	63%	42.7 mV	50.12 m ² g ⁻¹

Conductivity titration was used to quantitatively determine the amount of quaternary ammonium groups (i.e., the trimethylammonium chloride content in Table 1) and the degree of substitution in QNC samples. Zeta potential was also performed for measuring the overall charge density for wood pulp and QNC in the slurry or suspension form. From the conductivity titration study, no quaternary ammonium groups were observed from wood pulp (its zeta potential was -20.3 mV, Table 2). In contrast, both QNC 9:1-a and QNC 9:1-b samples exhibited a relatively high quaternary ammonium content $(0.327 \text{ to } 0.341 \text{ mmol g}^{-1}, \text{ respectively})$. The higher quaternary ammonium content in QNC 9:1-b might be due to the decreasing water content in the reaction. As the GTMAC ratio was increased to 12 to 1, the quaternary ammonium content increased to 0.486 mmol g⁻¹, corresponding to the degree of substitution equal to 0.078 mol mol⁻¹ AGU. These data match the zeta potential results, where all QNC samples showed positive surface charges with the following order: QNC 9:1a (27.9 mV) < QNC 9:1-b (36 mV) < QNC 12:1 (42.7 mV). Additionally, the zeta potential was also measured under different pH condition for the QNC 12:1 sample (Fig. S1, ESI†). The results showed that there was no significant change in the zeta potential value when the pH value was increased from 2 to 10. This indicates that the cationic quaternary ammonium groups in QNC remain relatively stable in a wide pH range. To understand the removal mechanism, we also performed the zeta potential measurement of QNC loaded with PFOA (Fig. S2, ESI†). In this study, 1.6 mL 0.03 wt% of QNC was firstly added into the small cuvette. Subsequently, 20, 40 and 60 μ l of 1g L⁻¹ PFOA was mixed with the QNC suspension, respectively, for certain time to reach equilibrium. It was found that zeta potential after PFOA adsorption decreased with the PFOA content from 38 mV to 10 mV. This observation indicates that the adoption of anionic PFAS molecules neutralize the cationic groups on QNC resulting in a lower surface charge of the scaffold, confirming that electrostatic interaction is the major adsorption mechanism by QNC for PFAS removal.

The XRD profiles for both wood pulp and QNC samples exhibited the cellulose I crystal structure (Fig. S3, ESI†). These profiles displayed three major diffraction peaks at 14.8°, 16.8° and 22.6°, indicating that cationization occurred mainly on the cellulose surface. There is no major difference in CI between the original pulp, QNC 9:1-a and 9:1-b samples, but the QNC 12:1 sample showed a lower CI value of 63% (Table 2). This observation is consistent with a previous study that the use of a large amount of GTMAC could result in converting crystalline microfibril structure into amorphous QNC derivatives.22 This

indicates at a lower GTMAC concentration, the cationization reagent tends to react with the amorphous cellulose chains first since their intermolecular force is relatively weak. As GTMAC concentration increases, the reagent begins to attach the crystalline chains resulting in the decrease in total crystallinity (as QNC 12:1).

The available surface area is an important parameter for the adsorption property. In this case, the solid samples' (air-dried wood pulp fiber and freeze-dried QNC samples) surface areas were measured by the BET technique, and results are shown in Table 2. It was seen that all QNC samples exhibited a much higher surface area compared with wood pulp (6.09 m² g⁻¹). The BET values in varying QNC samples can be explained by the degree of fibrillation. In specific, the comparison between the surface areas of ONC 9:1-a and 9:1-b indicate that the higher degree of quaternization leads to greater fibrillation, as expected. Surprisingly, the ONC 12:1 exhibited a lower surface area than QNC 9:1-b, which could have resulted from the excess dosage of GTMAC leading to some side reaction and the possible collapse of the scaffold structure during freeze-drying. We note that the surface area of QNC sample is not as high as those of solid porous materials, such as organosilica or GAC (average 400-600 m² g⁻¹).^{27,28} Again, this may reflect the fact that even with the freeze-drying technique, some nanocellulose scaffold may still collapse, resulting in a tighter porous network structure.

3.2. Batch adsorption studies for PFAS removal

3.2.1. Adsorption kinetics. The kinetic adsorption study was performed to evaluate the adsorption rate of different PFASs using the QNC 12:1 adsorbent (referred as QNC adsorbent hereinafter), where the results are shown in Fig. 3 (also Tables S5(a)-(d), ESI†). In Fig. 3a, it was seen that the adsorption equilibrium was achieved within 2 h for PFOA. In contrast, a significantly faster adsorption rate (99% removal within one minute) was observed for PFOS (Fig. 3c). For short-chain PFBA and PFBS, a relatively fast equilibrium (within 15 minutes) was also observed. However, sorption fluctuations were seen in the first two hours (Fig. 3b and d). These fluctuations are likely caused by the quasistatic sorption-desorption equilibrium between the weakly bonded short-chain PFAS and QNC in the initial sorption phase.29

Both pseudo-first order (eqn (1)) and pseudo-second order (eqn (2)) kinetic models were used to fit the kinetic data, where the fitting parameters are listed in Table 3. The expressions of these two models are as follow:28,30

$$\ln(q_{\text{e,exp}} - q_t) = \ln q_{\text{e,cal}} - k_1 t \tag{1}$$

$$\frac{t}{q_t} = \frac{1}{k_2 q_e^2} + \frac{t}{q_e} = \frac{1}{V_0} + \frac{t}{q_e}$$
 (2)

where q_e is the amount of PFAS adsorbed on QNC at the equilibrium (mg g $^{-1}$) ($q_{\rm e,exp}$ is the estimated value from the kinetic plot, $q_{e,cal}$ is the calculated value based on pseudo-first order), V_0 is the initial sorption rate (mmol $g^{-1} h^{-1}$), K_1 is the pseudofirst order sorption rate constant (h^{-1}), and K_2 is the pseudosecond order sorption rate constant (g mg⁻¹ h⁻¹).

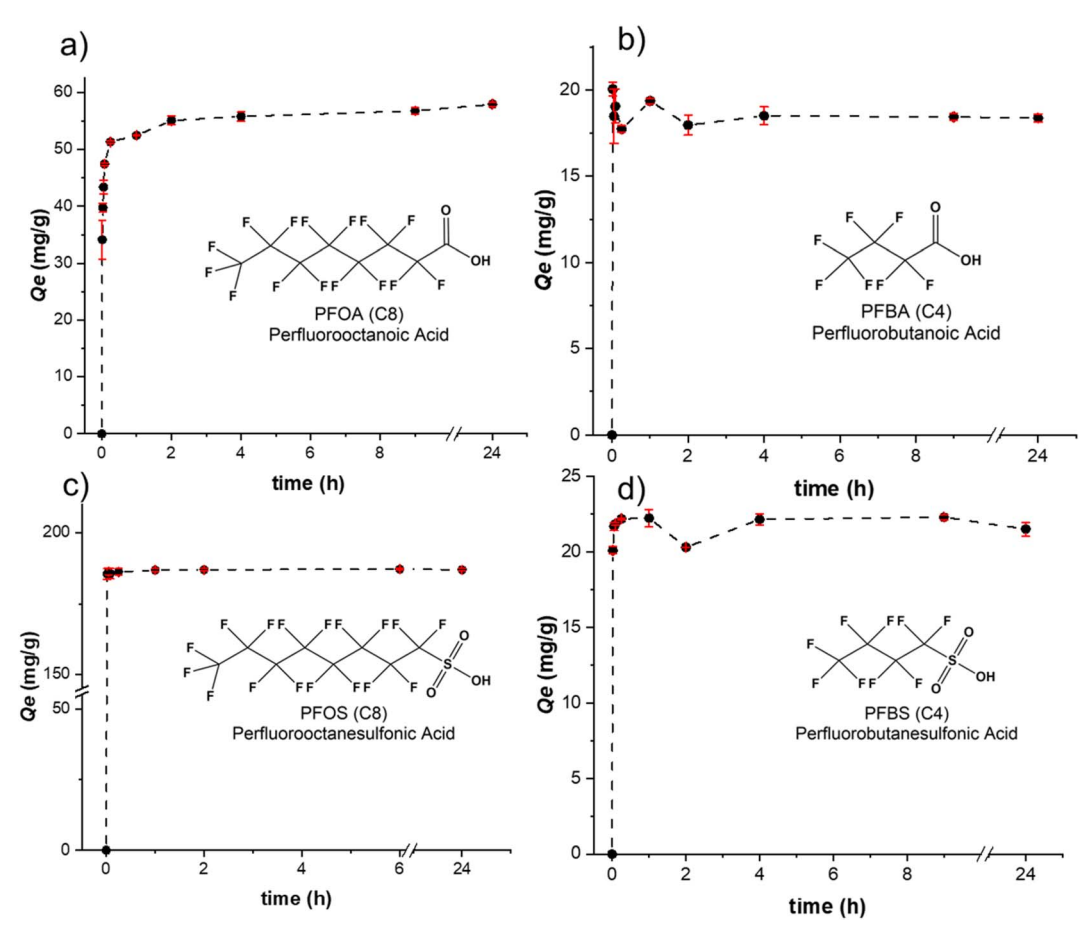


Fig. 3 The adsorption kinetic data of QNC gel against the removal of (a) PFOA; (b) PFBA; (c) PFOS; (d) PFBS over 24 h. The error bar was calculated from two replicates. The QNC concentration used was 32 mg L^{-1} for PFOA (2 mg L^{-1}) and PFOS (5 mg L^{-1}) or 320 mg L^{-1} for PFBA (10 mg L^{-1}) and PFBS (10 mg L^{-1}).

A higher fitting coefficient (R^2) obtained from the pseudo-second order fitting suggested that the PFAS sorption by QNC is probably controlled by chemical sorption.^{30,31} The initial sorption rate (V_0 , mmol g^{-1} h⁻¹) of the PFAS ranged from 2.2 mmol g^{-1} h⁻¹ to 50.4 mmol g^{-1} h⁻¹ for the PFAS examined (Table 3), *i.e.*, two orders of magnitude higher than the reported V_0 value for GAC (0.02–0.06 mmol g^{-1} h⁻¹), biochar (0.008–0.02 mmol g^{-1} h⁻¹)²⁸ and powdered activated carbon (PAC, 0.005–0.8 mmol g^{-1} h⁻¹).³² The initial uptake rate during the external diffusion step is directly related to a diffusion time

constant, D/Rad2, where D is the diffusivity of an adsorbate and Rad is the radius of the adsorbent.³³ The uptake of PFAS is expected to increase rapidly with decreasing adsorbent radius. It has been previously reported that GAC with 0.85–1.0 mm size could reach the equilibrium from 48 to 240 h, while PAC with 45–150 μ m size could reach the equilibrium within 2 h.³² As the average nanocellulose fiber dimensions were 110 \pm 57 nm in length and 6.5 \pm 1.4 nm in width (Fig. 2), it is not surprising to observe that QNC exhibited very fast initial PFAS sorption rates and very short equilibrium time for all chosen PFAS as shown in

Table 3 Pseudo-first order, pseudo-second order and intraparticle diffusion model fitting parameters from the kinetic adsorption data of QNC against different PFAS compounds^a

	Pseudo- first ord	ler model		Pseudo- secor	nd order model			Intraparticle diffusi model	ion
	$q_{ m e,cal}({ m mg~g^{-1}})$	K_1 (h^{-1})	R^2	$q_{ m e}~({ m mg~g}^{-1})$	$V_0 \text{ (mmol g}^{-1} \text{ h}^{-1}\text{)}$	K_2 (g mg ⁻¹ h ⁻¹)	R^2	$K_{\rm p} ({\rm mg \ g^{-1} \ h^{-0.5}})$	R^2
PFOA	10.96	0.29	0.70	57.97	2.2	0.27	0.99	51	0.84
PFBA	N.A.	N.A.	N.A.	19.42	15.69	8.84	0.99	18	N.A.
PFOS	1.25	1.04	0.84	187.3	50.4	7.17	0.99	186	0.78
PFBS	N.A.	N.A.	N.A.	22.29	2.64	1.60	0.99	21	0.11

^a N.A. means it is not applicable. The data can't be fitted by the model due to the large fluctuation.

Fig. 3. The nanoscale structure of QNC provides a very efficient PFAS sorption process (equilibrium within several minutes) when compared to conventional carbon-based adsorbents.

Additionally, the intra-particle diffusion model was also used to fit the kinetic data (Fig. 3), where the results are listed in Table 3. This model was based on the commonly adopted diffusion process, which has the following expression:²⁸

$$q_t = k_p \times t^{0.5} \tag{3}$$

where K_p (mg g⁻¹ h^{-0.5}) is the intra-particle diffusion rate constant. Due to the low fitting R^2 value (0.84–0.11), we felt the intra-particle model is not suitable to describe the kinetic data. This suggests the PFAS adsorption on QNC is not controlled by the intra-particle diffusion process.

The typical PFAS adsorption on general adsorbent consists of three processes: (i) external diffusion from bulk solution onto the adsorbent surface, (ii) intra-particle diffusion into the adsorbent pore, and (iii) instantaneous surface adsorption at the active sites (possibly fast and negligible).34 Unlike porous GAC, where the (ii) intra-particle diffusion process is the limiting step due to the small pore size (~ 1 nm), the QNC scaffold doesn't contain obvious porous structure (Fig. 2). From both Fig. 3 and Table 3, we argue the fast PFAS adsorption on QNC is very likely controlled by the (i) external diffusion process, which is supported by the high initial rate V_0 result. Therefore, the molecular size or steric effect of PFAS has less influence on the adsorption, where the kinetics mostly rely on the strength of interaction (electrostatic interaction) between PFAS and QNC. Overall, QNC showed faster kinetics for both long-chain and short-chain PFAS adsorption, and the equilibrium time was much shorter than those for GAC or even ionexchange resins, which usually are in the order of several days.28,35

3.2.2. Adsorption isotherm. To observe the adsorption capacity of QNC for different PFASs, isotherm study is shown in Fig. 4 (also Tables S6(a)-(d), ESI†). PFOS exhibited the highest equilibrium adsorption capacity (Q_e) of 550 mg g⁻¹ (1.1 mmol g^{-1}), followed by PFOA of 400 mg g^{-1} (0.97 mmol g^{-1}). It is well known that sulfonic acid is a stronger acid compared with carboxylic acid. Upon dissociation, the sulfonate group would exhibit a stronger anionic inductive effect than the carboxylate group. Also, a DFT modeling study has been carried out, where the results indicated that sulfonated PFAS has more negative exergonic energy than carboxylated PFAS.36 As a result, sulfonated PFAS could create stronger electrostatic interaction with cationic QNC than carboxylated PFAS.37 Additionally, PFOS (also PFBS) has one additional carbon in its hydrophobic tail than PFOA (and PFBA), which may further increase its hydrophobic interaction with QNC. The combined effect of electrostatic and hydrophobic interactions between PFOS and QNC resulted in the highest Qe value. Compared to long-chain PFOA/ PFOS, short-chain PFAS exhibited a lower equilibrium adsorption capacity: PFBS of 250 mg g⁻¹ (0.83 mmol g⁻¹) and PFBA of 100 mg g^{-1} (0.46 mmol g^{-1}). The above adsorption behavior is consistent with two published studies.3,38 A recent study39 indicated that the higher adsorption capacity for long-chain PFAS could be due to its micelle formation, depending on the critical micelle concentrations, which is also possible in our

In the study by Giles et al., they demonstrated that the isotherm data can be described as either the sigmoidal-shaped (S), Langmuir (L), high affinity (H), or constant partition (C) curve, depending on the initial slope and the curvature of the isotherm data.40 Both long-chain PFOS and PFOA isotherm data in Fig. 4 followed the H-curve, as they exhibited a sharp initial slope. In contrast, short-chain PFBS and PFBA isotherm data follow the L-curve having a less steep slope and a clear plateau value. The difference could be explained by the high affinity between long-chain PFAS and QNC as compared to short-chain PFAS and QNC. To quantitatively analyze the maximum adsorption capacity of ONC against PFAS, we used the common Langmuir (eqn (4)) and Freundlich (eqn (5)) models with the following expressions to fit the results in Fig. 4.

$$\frac{C_{\rm e}}{Q_{\rm e}} = \frac{1}{Q_{\rm m}K_{\rm L}} + \frac{C_{\rm e}}{Q_{\rm m}} \tag{4}$$

$$\log Q_{\rm e} = \log K_{\rm F} + \frac{1}{n} \log C_{\rm e} \tag{5}$$

where C_e is the equilibrium concentration of PFAS in mg L⁻¹, Q_e is the adsorbed PFAS amount (mg g^{-1}) at the equilibrium, $Q_{\rm m}$ (mg g⁻¹) represents the maximum Langmuir adsorption capacity, the Langmuir adsorption constant K_L (L g^{-1}) is positively related to the affinity of adsorption sites.30 In the Freundlich model, the Freundlich adsorption constant $K_{\rm F}$ (L^{1/n} $mg^{1-1/n}$ g^{-1}) indicates the adsorption capacity, where the n value affects the shape of curve. 30 The Langmuir model assumes the adsorption takes place on the surface as homogeneously mediated monolayer, where the Freundlich model assumes the

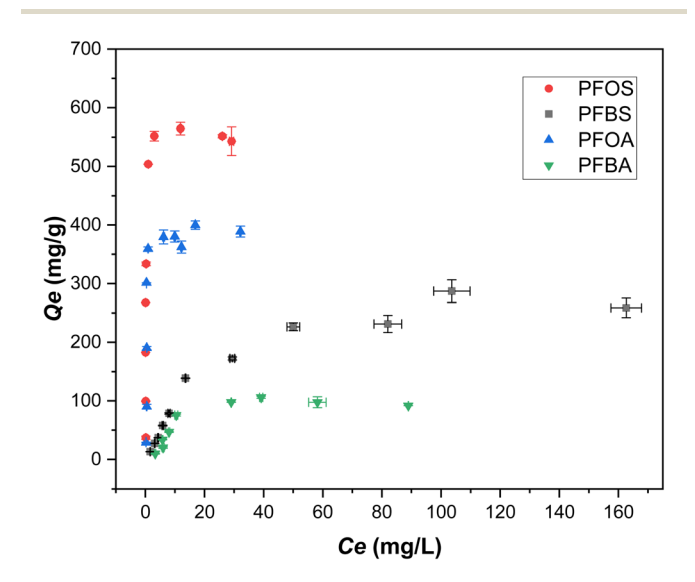


Fig. 4 Equilibrium adsorption capacity (Q_e) of the QNC 12:1 adsorbent versus equilibrium concentration (Ce) for four different PFAS (PFAS concentration: $1-50 \text{ mg L}^{-1}$ for PFOA and PFOS, $1-100 \text{ mg L}^{-1}$ for PFBA, 1-200 mg L^{-1} for PFBS; QNC concentration: 32 mg L^{-1} for PFOA and PFOS or 320 mg L^{-1} for PFBA and PFBS; equilibrium time; 24

Table 4 Langmuir and Freundlich model fitting parameters for different PFAS compounds a

	Langmuir mo	odel		Freundlich model		
	$Q_{\rm m} ({\rm mg \; g}^{-1})$	$K_{\rm L} \left({\rm L} \ {\rm g}^{-1} \right)$	R^2	$K_{\rm F} \left({\rm L}^{1/n} \ {\rm mg}^{1-1/n} \ {\rm g}^{-1} \right)$	n	R^2
PFOA	405	1.08	0.99	174	3.09	0.42
PFBA	121	0.058	0.85	9.34	1.63	0.69
PFOS	559	2.24	0.99	290	3.66	0.39
PFBS	319	0.037	0.97	15.67	1.56	0.90

 a The $Q_{\rm m}$ values from the Langmuir model were examined with the estimated highest $Q_{\rm e}$ values, where the difference was less than 10% making the result acceptable.

adsorption takes place on the surface as heterogeneously mediated multi-layer. The fitting parameters of the isotherm data using these two models are summarized in Table 4.

The fitting results by the Langmuir model showed a very good correlation ($R^2 = 0.85-0.99$) for all four PFASs, while the fitting by the Freundlich model was relatively poor ($R^2 = 0.39$ -0.90). To verify that there is a statistically significant difference between these two models, the one-tailed paired Student's t-test for R^2 values was carried out ($p \le 0.05$ means there is a statistically significant difference). The results showed that QNC has the highest $Q_{\rm m}$ (559 mg g⁻¹) and $K_{\rm L}$ values (2.24 L g⁻¹) for PFOS, but relatively lower $Q_{\rm m}$ (405 mg g⁻¹) and $K_{\rm L}$ values (1.08 L g⁻¹) for PFOA. Both Q_m values are considerably higher than the maximum adsorption capacity reported for GAC (236-480 mg g^{-1} against PFOS and 112–195 mg g^{-1} against PFOA). 41,42 On the other hand, the $Q_{\rm m}$ value for PFBS is 319 mg g⁻¹ and for PFBA is only 121 mg g⁻¹. However, these values are still higher than those of conventional GAC for short-chain PFASs (e.g., 9.3-98.7 mg g^{-1} for PFBS and 5.1-51.4 mg g^{-1} for PFBA) and ionexchange resins (34.6-109.2 mg g^{-1} for PFBS; 19.1-52.3 mg $\rm g^{-1}$ for PFBA). 28,35,41,42 The $\rm \textit{K}_{L}$ values for PFBA (0.0058 L $\rm g^{-1})$ and PFBS $(0.0037 \text{ L g}^{-1})$ are also much lower than those for longchain PFASs, confirming our notion that the adsorption affinity of short-chain PFAS by QNC is less than that of longchain PFAS by QNC.

3.2.3. Competition adsorption studies. Studying the competitive adsorption behavior between different types of PFAS towards QNC is critical for their effective removal. We performed two experiments to understand the competitive behavior among different PFASs: displacement study and competition study, where the results are displayed in Fig. 5 (also Tables S7(a), (b) for the displacement study, and Tables S8(a), (b) for the competition study, ESI†). In the displacement study, QNC was first saturated with short-chain PFAS, then long-chain PFAS was added after equilibrium. In the competition study, QNC was directly exposed to the mixture of long-chain and short-chain PFASs at the same concentration. We note that some previous studies were made to investigate the competitive adsorption between long-chain and short-chain PFASs in anionexchange resins. 43,44 These studies indicated that the increased pH value or increased PFAS concentration could induce shortchain PFAS replacement by long-chain PFAS,44 where the displacement trend depends on the PFAS molecular structure

and its hydrophobicity (*e.g.*, PFOS > PFHxS > PFOA > PFBS > PFHxA > PFBA).⁴³ Similar competition studies for bioadsorbents are seldom reported.

Due to the high adsorption capacity in QNC, the competitive phenomenon was not obvious at first when we used low concentration (10 mg L $^{-1}$) (Fig. 5e). After increasing the initial concentration gradually to 30 and 60 mg L $^{-1}$, the displacement behavior was seen, where the percentage of the $Q_{\rm e}$ decrease in short-chain PFAS became apparent. Specifically, when the displacement study was conducted at the condition of 160 mg L $^{-1}$ QNC with $\sim\!\!60$ mg L $^{-1}$ of PFAS, $Q_{\rm e}$ of PFBA decreased by 57% (from 128 mg g $^{-1}$ to 55 mg g $^{-1}$) after the introduction of PFOA (Fig. 5a). Similarly, the $Q_{\rm e}$ value of PFBS dropped by 65% (from 204 mg g $^{-1}$ to 72 mg g $^{-1}$) after PFOS was introduced (Fig. 5b). The whole displacement process happened within 5 min for the PFBS/PFOS system, where a slower equilibrium time (between 1 and 6 h) was observed for the PFBA/PFOA system.

The competition study also exhibited similar behavior when we mixed long-chain and short-chain PFASs simultaneously in the bisolute system. By comparing the results from single solute and bisolute systems in Fig. 5d, the Qe value of bisolute PFBS was much lower than that of single solute PFBS, while those of PFOS in bisolute and single solute systems remained the same. A similar trend was also discovered in the PFBA/PFOA mixture (Fig. 5c), but the Q_e difference of PFBA was much smaller than that of PFBS. Additionally, the Q_e value of PFOA was found to decrease slightly in bisolute system (Fig. 5f). Based on the above results, we conclude that long-chain PFAS is more easily adsorbed by QNC due to the combined electrostatic and hydrophobic interactions, whereas electrostatic interaction is the dominant mechanism for short-chain PFAS adsorption. Under this scenario, the displacement percentage is PFAS concentration dependent due to the availability of adsorption sites. These results indicate the challenge in short-chain PFAS removal was due to two reasons: (i) short-chain PFAS has much lower Q_m than long-chain PFAS because it lacks the hydrophobic aggregation ability; and (ii) once the adsorption reaches the limit, the adsorbed short-chain PFAS can be quickly displaced by long-chain PFAS.

Additionally, the following study was carried out to understand the PFAS selectivity by QNC and the competitive influence in the presence of background anions. In this study, NaCl was selected as the representative salt at extremely high level (0.1 M) and under an environmental relevant concentration (1 mM) (Fig. S4, Table S9, ESI†). It was surprising to observe that the PFOS adsorption was not impacted by the presence of high concentration of Cl⁻ ions at 0.1 M. There are few possible explanations for this observation. (1) Since PFOS has the highest hydrophobicity among four tested PFASs, it tends to form micelle or hemi-micelle with higher adsorption capacity. (2) High NaCl concentration could lead to salting-out effect, resulting in lower solubility for PFOS and thus better removal efficiency. (3) The electrostatic strength between PFOS and quaternary ammonium group on QNC is stronger than that with chloride ions. However, the removals of PFOA, PFBS and PFBA were found to decrease in the presence of anions, where the Q_e

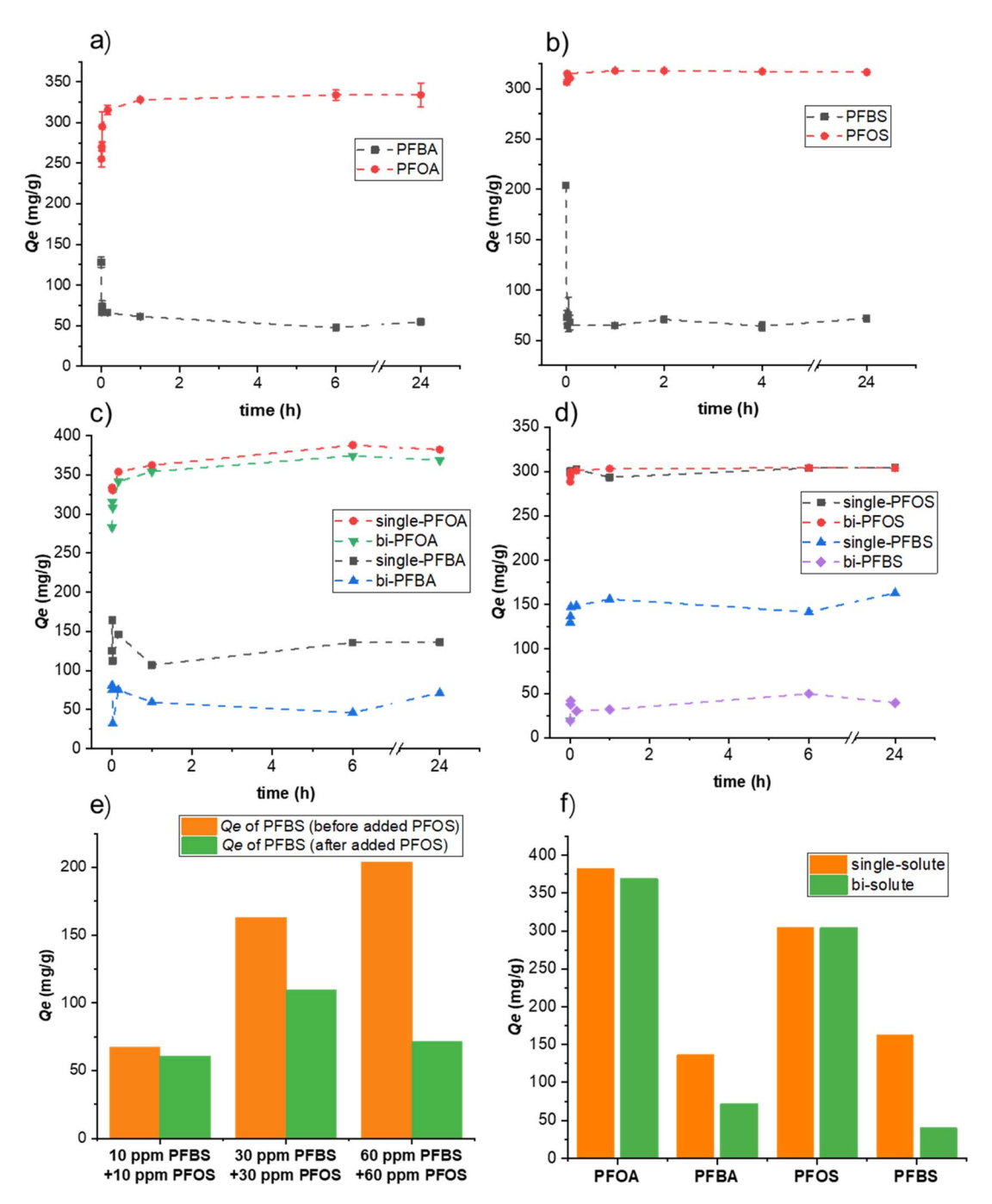


Fig. 5 The Q_e versus t plots in the displacement study of (a) PFBA-PFOA/and (b) PFBS- PFOS. (Short-chain PFAS was firstly mixed with QNC and reached equilibrium after 24 h, and then long-chain PFAS was added into the system. The time was recorded once the long-chain PFAS was introduced. The initial PFAS concentration was 60 mg L^{-1} , QNC concentration was 160 mg L^{-1}). The competition adsorption studies with single solute and bisolute matrix for (c) PFOA/PFBA and (d) PFOS/PFBS. (A mixture of long-chain and short-chain PFASs was added to QNC at the same time. The initial PFAS concentration was 60 mg L $^{-1}$, QNC concentration was 160 mg L $^{-1}$). (e) The histogram comparing the Q_e values at different PFAS concentrations in the displacement studies. (f) The histogram comparing the Q_e values for different PFAS in the competition studies.

of PFBA and PFBS even dropped to zero at 0.1 M of NaCl. Based on these results, we can conclude that the removal of shortchain PFASs are mostly via electrostatic adsorption process and are very sensitive to the background ions. In contrast, PFOS has the highest adsorption affinity with minimum impact in the presence NaCl.

3.3. Applications of QNC to treat PFAS-contaminated groundwater

To mimic the practical water treatment environment, contaminated groundwater sample was collected from Long Island, NY (Table S1, ESI†) and used to evaluate the effectiveness of QNC for PFAS removal. The results are shown in Table S2 (ESI†). It

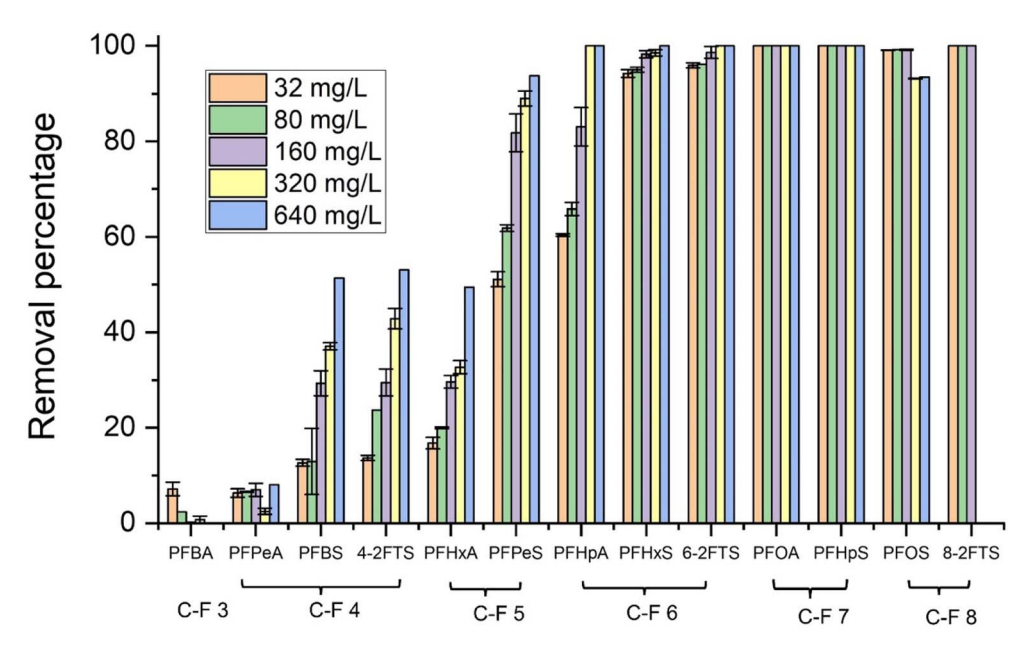


Fig. 6 Removal percentage of different PFASs in ground water sample by using various amounts of QNC (experimental condition: 9 ml ground water was mixed with 1 ml of QNC gel at 0.0032–0.064 wt% for 1 h).

was seen that the chosen groundwater sample contained 13 PFASs with total PFAS concentration of 11.7 $\mu g~L^{-1}$, in addition to various background ions and organics. In the QNC application study, we varied the amount of QNC adsorbent to remediate the PFAS level of the ground water sample for 1 h. A wood pulp sample without modification was also tested, where it did not exhibit any PFAS removal capability to treat this groundwater. In Table S2,† the bold numbers represent the final PFAS concentration that is below the detection limit (0.01 $\mu g~L^{-1}$) of the LC-MS/MS instrument, and those calculated results might be underestimated.

Overall, QNC showed excellent removal efficiencies (nearly 99%) for long-chain PFASs (C-F 7 and C-F 8) even at a low adsorbent concentration (32 mg L^{-1}) (Fig. 6). However, QNC only displayed moderate removal efficiencies (10-60%) for shorter chain-length PFASs (C-F 4 to C-F 6), where their removal performance increased with the increasing adsorbent dose. For example, the removal percentage of perfluoropentane sulfonic acid (PFPeS) and perfluoroheptanoic acid (PFHpA) reached >90% at 640 mg L^{-1} of QNC, while the removal of PFBS, 4:2 fluorotelomer sulfonic acid (4:2 FTS) and PFHxA reached only \sim 50% at the same QNC dose (640 mg L⁻¹). It was found that short-chain carboxylated PFAS, such as PFBA and PFPeA, were the most difficult components to be removed (<10%) even at the highest QNC concentration (640 mg L^{-1}). This may be due to their low adsorption affinity (carboxylate group) towards the QNC, combined with the interference effects (i.e., displacement and competition) between varying PFASs and other coconstituents (inorganic anions etc.) in groundwater. Another observation is that for PFASs with the same carbon number, sulfonate PFASs always showed better affinity to QNC than carboxylate PFASs (e.g., C-F 4 compounds removal, PFBS 13-51% and PFPeA 2-8%; C-F 5 compounds removal, PFPeS 5193% and PFHxA 17–49%). In addition, in the C–F 4 compound group, there is no significant removal difference between PFBS (13–51%) and 4:2 FTS (14–53%) (P > 0.05 in the T-test), indicating the influence of functional group is more profoundly than the influence of chain-length in this system. The overall adsorption trend is similar to other studies which also point out the challenge of PFBA removal. 36,45,46

4. PFAS removal mechanism by QNC

To-date, there are a great deal of studies regarding the PFAS removal mechanism, and it is well known that electrostatic interaction (ionic bonding) is much stronger than hydrophobic interactions (noncovalent bonding).14,15 The electrostatic interaction as the dominant PFAS removal mechanism has been reported in some cationic amine-containing organic adsorbents, which also exhibited the rapid PFAS removal kinetics. 19,20,36,47,48 Park et al. investigated the PFAS removal performance in magnetic ion-exchange resins to understand the role of the charge interaction.37 Surprisingly, PFOS and its branched isomer with different hydrophobicity showed almost equal equilibrium uptake due to their similar total atomic charge.49,52 The results clearly indicate that electrostatic interaction is the dominant force in the chosen magnetic ionexchange resin system, where the role of hydrophobic interaction is minor.37

As the QNC system in this study possesses plenty of cationic charged groups on surface so that electrostatic removal can be considered as primary driving force. However, the higher removal capacity for long-chain PFAS removal in isotherm study indicated that the hydrophobic attraction (due to van der Wall forces) also plays an important role. The results from the competition/displacement studies and the ground water test

Table 5 Summary and comparison of the maximum adsorption capacity and the molar ratio of short-chain/long-chain PFAS in relevant studies

)				
Adsorbent	Experimental condition	PFOA $Q_{\mathrm{m}}^{\ b}$	$\mathrm{PFBA}\ Q_{\mathrm{m}}^{\ b}$	Q_{m} molar ratio PFBA/PFOA	PFOS $Q_{\mathrm{m}}^{\ b}$	PFBS $Q_{ m m}^{\ b}$	$Q_{ m m}$ molar ratio PFBS/PFOS	Ref
Synthetic materials Quaternized nanocellulose (QNC)	Adsorbent dose = 32 mg L ⁻¹ (PFOA and PFOS) or 320 mg L ⁻¹ (PFBA and PFBS); Co = 1- 50 mg L ⁻¹ (PFOA and PFOS), 1-	405 mg g^{-1} $(0.98 \text{ mmol g}^{-1})$	121 mg g ⁻¹ $(0.57 \text{ mmol g}^{-1})$	0.58	559 mg g $^{-1}$ (1.12 mmol g $^{-1}$)	319 mg g^{-1} (1.06 mmol g^{-1})	0.95	Our work
Aminated rice husk Covalent triazine-based framework	(PFBS) Adsorbent dose = 100 mg L^{-1} ; Co = 0-0.5 mmol L ⁻¹ ; Adsorbent dose = 250 mg L^{-1} ; 3.8-259 mg L ⁻¹ (PFOA), 59.9-415 mg L ⁻¹ (PFOS),	1031 mg g ⁻¹ (2.49 mmol g ⁻¹) 269 mg g ⁻¹ (0.65 mmol g ⁻¹)	364 mg g ⁻¹ (1.7 mmol g ⁻¹) 92 mg g ⁻¹ (0.43 mmol g ⁻¹)	0.68	1325 mg g ⁻¹ (2.65 mmol g ⁻¹) 665 mg g ⁻¹ (1.33 mmol g ⁻¹)	N.A. ^a 141 mg g ⁻¹ $(0.47 \text{ mmol g}^{-1})$	N.A." 0.35	39
Organically modified silica (poly-SOMS) Zirconium-based	6.5-204 mg L ⁻ (PFBA), 6-247 mg L ⁻¹ (PFBS) Adsorbent dose = 40 mg L ⁻¹ ; Co = 0.25-2 mg L ⁻¹ Adsorbent dose = 200 mg L ⁻¹ ;	12.7 mg g ⁻¹ (0.031 mmol g ⁻¹) ^c 507 mg g ⁻¹	5.7 mg g ⁻¹ $(0.027 \text{ mmol g}^{-1})^c$ 274 mg g ⁻¹	0.87	8.9 mg g ⁻¹ (0.018 mmol g ⁻¹) ^c 622 mg g ⁻¹	7.7 mg g ⁻¹ (0.026 mmol g ⁻¹) ^c 404 mg g ⁻¹	1.44	27
framework Carbonaceous materials AC Calgon 3.8 415 204	rerials Adsorbent dose = 250 mg L^{-1} ; $3.8^{-2.59} \text{ mg L}^{-1}$ (PFOA), 59.9^{-1} 415 mg L ⁻¹ (PFOS), 6.5^{-1} 204 mg L ⁻¹ (PFBA), 6.247 mg L^{-1}	$(0.47 \text{ mmol g}^{-1})$	51.36 mg g^{-1} $(0.24 \text{ mmol g}^{-1})$	0.51	480 mg g ⁻¹ $(0.96 \text{ mmol g}^{-1})$	51 mg g^{-1} $(0.17 \text{ mmol g}^{-1})$	0.18	41
GAC Calgon 400 GAC Calgon F- 600 GAC Biochar	(PFBS) Adsorbent dose = 1000 mg L^{-1} ; Co = $15-150 \text{ mg L}^{-1}$ Adsorbent dose = 20 2000 mg L^{-1} ; Co = 50 mg L^{-1} ; Adsorbent dose = 50 mg L^{-1} ; Co = $0.1-1 \text{ mg L}^{-1}$; Adsorbent dose = 50 mg L^{-1} ; Co = $0.1-1 \text{ mg L}^{-1}$; Co = $0.1-1 \text{ mg L}^{-1}$;	112.1 mg g ⁻¹ (0.27 mmol g ⁻¹) 76.1 mg g ⁻¹ (0.18 mmol g ⁻¹) 35.6 mg g ⁻¹ (0.086 mmol g ⁻¹) 21.5 mg g ⁻¹ (0.052 mmol g ⁻¹)	NA. 15.3 mg g ⁻¹ (0.071 mmol g ⁻¹) ^d 5.1 mg g ⁻¹ (0.024 mmol g ⁻¹) 10.3 mg g ⁻¹ (0.048 mmol g ⁻¹)	N.A. 0.39 0.28 0.92	236.4 mg g ⁻¹ (0.47 mmol g ⁻¹) 81.3 mg g ⁻¹ (0.16 mmol g ⁻¹) ^d 60 mg g ⁻¹ (0.12 mmol g ⁻¹) 35 mg g ⁻¹	98.7 mg g ⁻¹ (0.33 mmol g ⁻¹) 40 mg g ⁻¹ (0.13 mmol g ⁻¹) 9.3 mg g ⁻¹ (0.031 mmol g ⁻¹) 6.9 mg g ⁻¹	0.70 0.81 0.26 0.33	42 50 28 28
Ion-exchange resins IRA 910 A600E	Adsorbent dose = 100 mg L^{-1} ; Co = $50\text{-}400 \text{ mg L}^{-1}$ Adsorbent dose = 1000 mg L^{-1} ; Co = 1000 mg L^{-1} ;	1436.6 mg g ⁻¹ $(3.47 \text{ mmol g}^{-1})$ 125.2 mg g ⁻¹ $(0.30 \text{ mmol g}^{-1})^f$	635.7 mg g ⁻¹ (2.97 mmol g ⁻¹) 19.1 mg g ⁻¹ (0.089 mmol g ⁻¹ $)$	0.86	1395 mg g ⁻¹ (2.79 mmol g ⁻¹) ^{ℓ} (0.37 mmol g ⁻¹) ^{ℓ}	1023.3 mg g ⁻¹ (3.41 mmol g ⁻¹) 34.6 mg g ⁻¹ (0.12 mmol g ⁻¹ $)$	1.22	43 35

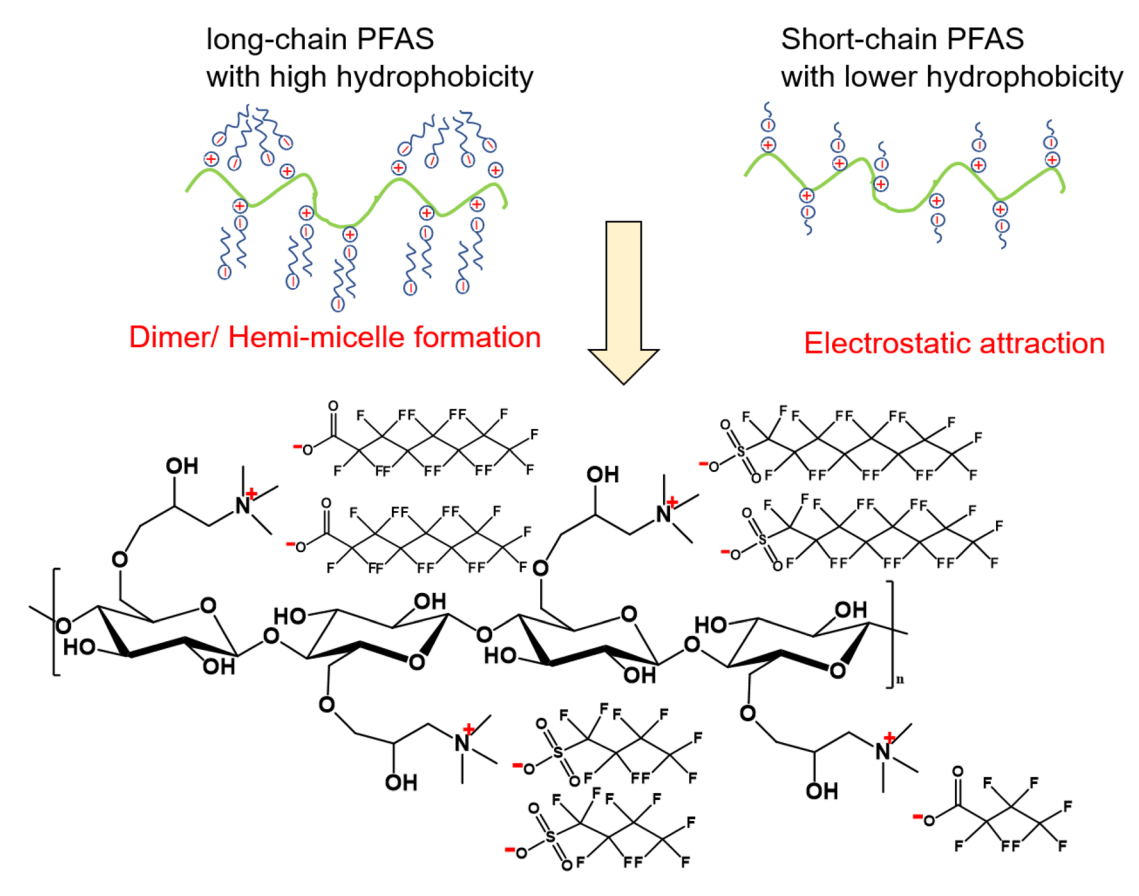
Table 5 (Contd.)

Adsorbent	Experimental condition	PFOA $Q_{\mathrm{m}}^{\ \ b}$	PFBA $Q_{ m m}^{\ \ b}$	Q_{m} molar ratio PFBA/PFOA PFOS $Q_{\mathrm{m}}^{\ b}$	PFOS $Q_{\mathrm{m}}^{\ b}$	PFBS $Q_{ m m}^{\ b}$	Q _m molar ratio PFBS/PFOS	Ref
A520E	Adsorbent dose = 1000 mg L^{-1} ;	134.7 mg g^{-1}	29.5 mg g ⁻¹	0.42	210.4 mg g^{-1}	53.8 mg g ⁻¹ (0.19 mmol g^{-1})	0.43	35
A532E	$CO = 1000 \text{ mg L}^{-1}$; Adsorbent dose = 1000 mg L^{-1} ; $CO = 1000 \text{ mg L}^{-1}$	(0.35 mmod g) 142.1 mg g^{-1} $(0.34 \text{ mmol g}^{-1})^f$	(0.14 mmol g) 52.3 mg g^{-1} $(0.24 \text{ mmol g}^{-1})^f$	0.72	(0.42 mmol g) 260.5 mg g^{-1} $(0.52 \text{ mmol g}^{-1})f$	(0.36 mmol g) 109.2 mg g^{-1} $(0.36 \text{ mmol g}^{-1})$	69.0	35

N.A. means there is no data available for specific PFAS. b The Q_{\max} values are derived from Langmuir fitting result, unless otherwise noted. c The Q_e value was calculated at $G_e = 200 \, \mu \mathrm{g} \, \mathrm{L}^{-1}$ using the Freundlich fitting model. ^d The Q_{max} value was estimated from the BET isotherm model. ^e The Langmuir correlation (R² = 0.71) was poor for PFOS in IRA 910. ^f The Q_e value was estimated based on the adsorption curve at the equilibrium clearly indicate that long-chain PFASs have better adsorption affinity than short-chain PFASs towards the QNC adsorbent due to additional hydrophobic interaction. The ion test confirmed that short-chain PFASs are easily affected by the presence of other anions as their dominant mechanism is electrostatic adsorption. In the groundwater test containing multiple PFAS mixtures, the PFBA removal capacity was the lowest, indicating that electrostatic attraction between the carboxylate group in PFAS and ammonium group on QNC was lower than that between the sulfonate group in PFAS and QNC.

The maximum adsorption capacity $Q_{\rm m}$ in the molar unit mmol g^{-1} (instead of the weight unit mg g^{-1}) is an important measure to understand the removal mechanism, as the value reflects the amount of the functional group on QNC. According to the conductivity titration result in Table 1, the amount of quaternary ammonium group (NR₄⁺) is 0.486 mmol g⁻¹ for the tested QNC adsorbent (QNC 12:1). It is surprising to notice that PFOS (1.12 mmol g⁻¹), PFBS (1.06 mmol g⁻¹) and PFOA (0.98 mmol g⁻¹) showed similar $Q_{\rm m}$ values in the molar unit, which is close to 1.0 mmol g^{-1} or about a 2:1 ratio when compared to the content of NR_4^+ group (Table 5). However, Q_m of PFBA is only 0.57 mmol g⁻¹, which is 1:1 to the NR₄⁺ group and indicates that the adsorption is mainly by electrostatic attraction between the two. One recent study of ion-exchange resin IRA 910 showed similar results, where adsorbed PFAS and released chloride ratio was measured to elucidate the adsorption mechanism for each PFAS. 43 The PFBA with chloride ratio was found to be 1, while all other long-chain PFASs exhibited a ratio larger than 1.43 Since PFBS, PFOA and PFBS are more hydrophobic than PFBA, we hypothesize that the hydrophobic interaction between PFAS molecules, forming a dimer or small aggregation (e.g. hemi-micelle) structure with one PFAS molecule tethered to the QNC backbone, may be a possible pathway to enhance the adsorption capacity. The proposed mechanism is shown in Fig. 7. Unfortunately, we do not have any further experimental results (such as scattering) to support this hypothesis. When comparing PFOA and PFBS, the effect of functional group might offset the effect of chain-length (PFOA: longer chain and weaker functional group: PFBS: shorter chain but stronger functional group), thus yielding the similar adsorption capacity. This phenomenon also indicates that in the electrostatic interaction driven system like QNC, the role of functional groups on PFAS weighs more than the role of hydrophobicity affecting the adsorption capacity. This hypothesis is also supported by the groundwater result. As PFBA has the lowest hydrophobicity and lowest electrostatic affinity among four tested PFASs, PFBA showed the lowest adsorption capacity by QNC since it can only be removed by electrostatic interaction. 36,48 Nevertheless, $Q_{\rm m}$ of PFBA on QNC (121 mg g⁻¹) is still higher than most of non-charged adsorbents such as GAC and biochar (5.1-51.36 mg g⁻¹) (Table 5), supporting that electrostatic interaction is beneficial to short-chain PFAS removal.

In addition to evaluating the maximum adsorption capacity, we have also compared the molar ratio of $Q_{\rm m}$ (close to $Q_{\rm e}$) between short-chain (C4) and long-chain (C8) PFASs using different adsorbents in the relevant studies, where the results



The proposed adsorption mechanism of long-chain and short-chain PFASs by the QNC adsorbent.

are summarized in Table 5. In this table, the $Q_{\rm m}$ molar ratio can provide the benchmark to evaluate the short-chain PFAS adsorption capacity for each adsorbent relative to their longchain analogues. In principle, the available adsorption sites on the adsorbent are fixed, so the difference in the removal capacity for each PFAS compound is only related to their sorption affinity. The higher molar ratio of $Q_{\rm m}$ between short-chain and long-chain PFAS indicates that the sorption affinity between the two becomes more similar. As seen in Table 5, the maximum adsorption capacity of short-chain PFASs are rarely reported to surpass their long-chain counterparts. However, the Qm molar ratio of short-chain/long-chain PFASs can often reach close to 0.7-0.9 as a good standard. There are some exceptions for organically modified silica and exchange resin (IRA 910), whose PFBS/PFOS ratio is larger than 1.0. This may be because the $Q_{\rm m}$ in the silica study was too low, and the correlation of the Langmuir model for PFOS in the IRA 910 study was poor $(R^2 =$ 0.71), rendering the calculated ratio values unreliable.

In Table 5, the chosen adsorbents can be classified into three categories: synthetic materials (containing bioadsorbents), carbonaceous materials, and ion-exchange resins. In synthetic materials, the corresponding Q_m mole ratios of short-chain/ long-chain PFASs are relatively high. For example, aminated rice husk shows high Q_m values for both long-chain and shortchain PFASs, leading to a Q_m molar ratio of PFBA/PFOA of 0.68. This can be attributed to the abundant cationic charge groups

on the adsorbent surface.³⁹ Our current study yielded results similar to the study of aminated rice husk: the $Q_{\rm m}$ molar ratio of PFBA/PFOA only reached 0.58, while that of PFBS/PFOS was 0.95, suggesting that the sorption affinity in short-chain sulfonated PFBS was also high. Zirconium-based metalorganic framework (NU-1000) was another successful example that used electrostatic interactions to remove PFAS effectively. 49 The adsorbent showed similar removal for both long-chain and short-chain PFAS (adsorption molar ratio was ~1.0), and the primary adsorption mechanism was anion exchange reaction at the metal node. For GAC and biochar materials, their $Q_{\rm m}$ values are moderate for long-chain PFAS but relatively low for shortchain PFAS (PFBA and PFBS), resulting in low Q_m molar ratios of short-chain PFAS versus long-chain PFAS. This result can be expected because the hydrophobic interaction is the major mechanism in activated carbons, where the adsorption and process of short-chain PFAS aggregation becomes unlikely due to the reduced hydrophobicity. In the case of ion-exchange resins, the Q_m molar ratios of short-chain/long-chain PFAS varied and did not show a clear trend. Perhaps this is because its $Q_{\rm m}$ value is strongly influenced by the polymeric backbone and available functional groups. For instance, Zaggia et al. compared three ion-exchange resins with different hydrophobicity, and it was found that the resin A532E with more hydrophobic functional groups exhibited higher adsorption capacity for both long-chain and short-chain PFAS than A520E (fairly

hydrophobic) and A600E (non-hydrophobic). The increased hydrophobicity in A532E led to a high $Q_{\rm m}$ value for short-chain PFAS adsorption, rendering higher $Q_{\rm m}$ molar ratios of short-chain/long-chain PFAS (0.72 for PFBA/PFOA and 0.69 for PFBS/PFOS).³⁵ In the case of IRA 910, an ion-exchange resin containing polystyrene-divinylbenzene backbone and dimethyl ethanol ammonium group, it showed very high $Q_{\rm m}$ values for all four PFASs yielding a high $Q_{\rm m}$ molar ratio of short-chain/long-chain PFAS (0.86 for PFBA/PFOA).⁴³ Based on the results from Table 5, we conclude that synthetic materials with high charge density and ion-exchange resins are more effective than carbonaceous materials for short-chain PFAS removal, due to higher electrostatic interactions between PFAS and adsorbent.

5. Conclusions

The current study demonstrates the development of a cationic quaternized nanocellulose (QNC) adsorbent system, which is potentially low cost, sustainable and effective to remove a wide range of long-chain and short-chain PFAS molecules. This is because the availability of abundant cationic sites (quaternary ammonium groups) and the large surface area in QNC facilitate both electrostatic and hydrophobic interactions with anionic PFAS molecules, resulting in fast removal kinetics and high removal capacity. The major findings can be summarized as below:

- (I) From the adsorption isotherm study, the calculated maximum adsorption capacity results (expressed in the molar unit) indicate that the adsorbed long-chain PFAS molecules may induce a dimer or small aggregation (hemi-micelle) structure with other PFAS molecules, resulting in higher values. In contrast, the maximum adsorption capacity of PFBA and the results from the NaCl ion test indicate that electrostatic interaction is the only driving force for the adsorption of PFBA onto the cationic sites in QNC.
- (II) Both displacement and competition studies indicate that short-chain PFASs could be easily displaced by their long-chain counterparts, where the competitive level is also dependent on the initial PFAS concentration.
- (III) Using a groundwater sample collected on Long Island, New York, the demonstrated QNC system effectively removed most PFASs, with the exception of carboxylated short-chain PFASs, such as PFBA and PFPeA.

This work demonstrated the importance of electrostatic interaction in terms of enhanced short-chain PFAS removal, according to relatively higher adsorption amount and molar ratio (short-chain *versus* long-chain) as compared to conventional GAC system. We believe the QNC system can outperform most of synthetic adsorbents and ion-exchange polymers in many aspects, such as sustainability and performance/cost ratio. However, the strategy to improve the removal efficiency against carboxylated short-chain PFASs ($C \le 4$) will still need to be developed to take advantage of the unique nature of nanocellulose scaffolds. Some perspectives include utilized synergistic effects by combining electrostatic interaction with hydrophobic or fluor–fluor interactions.^{27,46,50,51}

In terms of practical applications, unlike conventional adsorbents, QNC itself is relatively low-cost, biodegradable, and environmentally friendly. As a result, the used samples can be safely destroyed without the need for expensive regeneration of the adsorbent. The destruction techniques may include the methods of plasma, electron beam and electrochemistry. To ensure the safe handling of nanomaterials for industrial applications, post cross-linking method or solidification methods can be further used to ensure the use of nanocellulose as adsorbent media. QNC represents a new class of PFAS remediation material, which provides complementary property when compared with other effective adsorbents (e.g., GAC, ion exchange resins, and MOF). It is conceivable QNC can be used in combination with these adsorbents in a sequential manner to achieve more effective PFAS removal efficiency.

Conflicts of interest

There are no conflicts to declare.

Acknowledgements

The authors acknowledge the financial support of this work by the Division of Chemical, Bioengineering, Environmental and Transport Systems (CBET-2052772) and the Division of Materials Science (DMR-2216585) of the US National Science Foundation.

References

- 1 R. C. Buck, J. Franklin, U. Berger, J. M. Conder, I. T. Cousins, P. de Voogt, A. A. Jensen, K. Kannan, S. A. Mabury and S. P. van Leeuwen, *Integr. Environ. Assess. Manag.*, 2011, 7, 513–541.
- 2 B. Kuehn, J. Am. Med. Assoc., 2019, 322, 1757.
- 3 F. Li, J. Duan, S. Tian, H. Ji, Y. Zhu, Z. Wei and D. Zhao, *Chem. Eng. J.*, 2020, **380**, 122506.
- 4 O. U. G. P. Group, *Synthesis Paper on Per- and Polyfluorinated Chemicals (PFCs)*, Health and Safety Environment, Environment Directorate, Paris, 2013.
- 5 C. T. Vu and T. Wu, *Environ. Sci. Water Res. Technol.*, 2020, 6, 2958–2972.
- 6 K. Loria, *Dangerous PFAS Chemicals Are in Your Food Packaging*, Consumer Reports, 2022.
- 7 P. Grandjean, C. A. G. Timmermann, M. Kruse, F. Nielsen, P. J. Vinholt, L. Boding, C. Heilmann and K. Mølbak, *PLoS One*, 2020, 15, e0244815.
- 8 M. Nian, K. Luo, F. Luo, R. Aimuzi, X. Huo, Q. Chen, Y. Tian and J. Zhang, *Environ. Sci. Technol.*, 2020, 54, 8291–8299.
- 9 E. Marques, M. Pfohl, W. Wei, G. Tarantola, L. Ford, O. Amaeze, J. Alesio, S. Ryu, X. Jia, H. Zhu, G. D. Bothun and A. Slitt, *Toxicol. Appl. Pharmacol.*, 2022, 442, 115991.
- 10 K. Londhe, C.-S. Lee, Y. Zhang, S. Grdanovska, T. Kroc, C. A. Cooper and A. K. Venkatesan, ACS ES&T Eng., 2021, 1, 827–841.

- 11 I. Ross, J. McDonough, J. Miles, P. Storch, P. Thelakkat Kochunarayanan, E. Kalve, J. Hurst, S. S. Dasgupta and J. Burdick, Remed. J., 2018, 28, 101-126.
- 12 A. K. Venkatesan, C.-S. Lee and C. J. Gobler, Sci. Total Environ., 2022, 847, 157577.
- 13 M. Park, S. Wu, I. J. Lopez, J. Y. Chang, T. Karanfil and S. A. Snyder, Water Res., 2020, 170, 115364.
- 14 Z. Du, S. Deng, Y. Bei, Q. Huang, B. Wang, J. Huang and G. Yu, J. Hazard. Mater., 2014, 274, 443-454.
- 15 D. Banks, B.-M. Jun, J. Heo, N. Her, C. M. Park and Y. Yoon, Sep. Purif. Technol., 2020, 231, 115929.
- 16 D. Q. Zhang, W. L. Zhang and Y. N. Liang, Sci. Total Environ., 2019, 694, 133606.
- 17 P. Ganguly, A. Breen and S. C. Pillai, ACS Biomater. Sci. Eng., 2018, 4, 2237-2275.
- 18 R. Das, T. Lindstrom, P. R. Sharma, K. Chi and B. S. Hsiao, Chem. Rev., 2022, 8936-9031.
- 19 D. Li, K. Londhe, K. Chi, C. S. Lee, A. K. Venkatesan and B. S. Hsiao, AWWA Water Sci., 2021, 3, e1258.
- 20 J. T. Harris, G. D. de la Garza, A. M. Devlin and A. J. McNeil, ACS ES&T Water, 2022, 2, 349-356.
- 21 H. Sehaqui, A. Mautner, U. Perez de Larraya, N. Pfenninger, P. Tingaut and T. Zimmermann, Carbohydr. Polym., 2016, **135**, 334-340.
- 22 A. Pei, N. Butchosa, L. A. Berglund and Q. Zhou, Soft Matter, 2013, 9, 2047.
- 23 S. Saini, C. Yucel Falco, M. N. Belgacem and J. Bras, Carbohydr. Polym., 2016, 135, 239-247.
- 24 M. Zaman, H. Xiao, F. Chibante and Y. Ni, Carbohydr. Polym., 2012, 89, 163-170.
- 25 T. Kolev, M. Spiteller and B. Koleva, Amino Acids, 2010, 38, 45-50.
- 26 A. R. Katritzky, J. Am. Chem. Soc., 1996, 118, 3543.
- 27 E. K. Stebel, K. A. Pike, H. Nguyen, H. A. Hartmann, M. J. Klonowski, M. G. Lawrence, R. M. Collins, C. E. Hefner and P. L. Edmiston, Environ. Sci. Water Res. Technol., 2019, 5, 1854-1866.
- 28 D. Zhang, Q. He, M. Wang, W. Zhang and Y. Liang, Environ. Technol., 2021, 42, 1798-1809.
- 29 P. McCleaf, S. Englund, A. Ostlund, K. Lindegren, K. Wiberg and L. Ahrens, Water Res., 2017, 120, 77-87.
- 30 Q. Hu, Q. Wang, C. Feng, Z. Zhang, Z. Lei and K. Shimizu, J. Mol. Liq., 2018, 254, 20-25.
- 31 Y. S. Ho and G. McKay, Process Biochem., 1999, 34, 451-465.

- 32 Y. Zhi and J. Liu, Environ. Pollut., 2015, 202, 168-176.
- 33 R. T. Yang, Adsorbents: Fundamentals and Applications, John Wiley & Sons, Inc., 2003.
- 34 P. Chingombe, B. Saha and R. J. Wakeman, J. Colloid Interface Sci., 2006, 302, 408-416.
- 35 A. Zaggia, L. Conte, L. Falletti, M. Fant and A. Chiorboli, Water Res., 2016, 91, 137-146.
- 36 M. Ateia, M. Arifuzzaman, S. Pellizzeri, M. F. Attia, N. Tharayil, J. N. Anker and T. Karanfil, Water Res., 2019, 163, 114874.
- 37 M. Park, K. D. Daniels, S. Wu, A. D. Ziska and S. A. Snyder, Water Res., 2020, 181, 115897.
- 38 E. Gagliano, M. Sgroi, P. P. Falciglia, F. G. A. Vagliasindi and P. Roccaro, Water Res., 2020, 171, 115381.
- 39 S. Deng, L. Niu, Y. Bei, B. Wang, J. Huang and G. Yu, Chemosphere, 2013, 91, 124-130.
- 40 C. H. Giles, D. Smith and A. Huitson, I. Colloid Interface Sci., 1974, 47, 755-765.
- 41 B. Wang, L. S. Lee, C. Wei, H. Fu, S. Zheng, Z. Xu and D. Zhu, Environ. Pollut., 2016, 216, 884-892.
- 42 V. Ochoa-Herrera and R. Sierra-Alvarez, Chemosphere, 2008, 72, 1588-1593.
- 43 A. Maimaiti, S. Deng, P. Meng, W. Wang, B. Wang, J. Huang, Y. Wang and G. Yu, Chem. Eng. J., 2018, 348, 494-502.
- 44 W. Wang, X. Mi, Z. Zhou, S. Zhou, C. Li, X. Hu, D. Qi and S. Deng, J. Colloid Interface Sci., 2019, 557, 655-663.
- 45 H. Son, T. Kim, H.-S. Yoom, D. Zhao and B. An, Water, 2020,
- 46 X. Min and Y. Wang, J. Hazard. Mater., 2023, 449, 131047.
- 47 W. Ji, L. Xiao, Y. Ling, C. Ching, M. Matsumoto, R. P. Bisbey, D. E. Helbling and W. R. Dichtel, J. Am. Chem. Soc., 2018, 140, 12677-12681.
- 48 E. Kumarasamy, I. M. Manning, L. B. Collins, O. Coronell and F. A. Leibfarth, ACS Cent. Sci., 2020, 6, 487-492.
- 49 R. Li, S. Alomari, R. Stanton, M. C. Wasson, T. Islamoglu, O. K. Farha, T. M. Holsen, S. M. Thagard, D. J. Trivedi and M. Wriedt, Chem. Mater., 2021, 33, 3276-3285.
- 50 X. Tan, M. Sawczyk, Y. Chang, Y. Wang, A. Usman, C. Fu, P. Král, H. Peng, C. Zhang and A. K. Whittaker, Macromolecules, 2022, 55, 1077-1087.
- 51 Q. Dong, X. Min, J. Huo and Y. Wang, Chem. Eng. J. Adv., 2021, 7, 100135.
- 52 K. Londhe, C. S. Lee, C. A. McDonough and A. K. Venkatesan, Environ. Sci. Technol., 2022, 56(22), 15207-15219.